Robotica (2014) volume 32, pp. 1191–1211. © Cambridge University Press 2014
doi:10.1017/S0263574714001945

Optimization and analysis of a redundant 4R spherical wrist mechanism for a shoulder exoskeleton

Ho Shing Lo* and Shengquan Xie

Department of Mechanical Engineering, University of Auckland, Auckland, New Zealand

(Accepted June 19, 2014. First published online: July 17, 2014)

SUMMARY

This paper presents a redundant 4-revolute (4R) spherical wrist mechanism for a shoulder exoskeleton, which overcomes several major issues with the 3R mechanisms used in the past. An analysis of the 3R mechanism is done to highlight the limitations in its range of motion and problems caused by operating near singular configurations. To ensure that the redundancy in the 4R mechanism is efficiently utilized, genetic algorithm is used to optimize the mechanism design and identify the optimal operating configurations of the mechanism. The capability to reach the entire shoulder workspace is guaranteed and the joint velocities are minimized by considering the joint displacements required to move the end-effector throughout the workspace and the condition number of joint configurations for reaching 89 positions in the workspace. Analysis of the 4R mechanism obtained from the optimization process indicates that it can move throughout the entire shoulder workspace with feasibly low joint velocities.

KEYWORDS: Exoskeletons; Rehabilitation; Redundant manipulators; Design optimization; Workspace analysis; Singularity analysis.

1. Introduction

Upper limb exoskeletons developed in the past have limitations in the shoulder mechanism which cause restrictions in the shoulder movement and prevent the exoskeleton from achieving the entire range of motion of the human shoulder. These exoskeletons commonly use a 3-revolute (3R) spherical wrist mechanism with two 90° links to produce spherical movements of the human shoulder joint.[1–6] The basic structure of these 3R exoskeletons is shown in Fig. 1, where the most distal third joint is implemented using a revolving mechanism around the upper arm. A problem arising from using the 3R mechanism is that it has singular configurations in which two of the rotary joints align with each other resulting in the loss of 1 degree-of-freedom (DOF).[1–4,7] When the 3R mechanism approaches a singular configuration, the mechanism has difficulty performing rotations about the axis that is lost. A small rotation of the shoulder about the lost axis requires high velocities from 3R joints. The worst case is when two of the 3R joints completely align with each other, i.e. a singular configuration occurs as shown in Fig. 1. In this situation, the 3R mechanism needs to change its configuration to produce rotations about the lost axis (Fig. 2).

The design shown in Fig. 1 is the simplest design of the 3R exoskeleton with the base joint of the 3R mechanism positioned directly behind the shoulder. In addition to the singularity problem, this exoskeleton design has a limited range of motion due to the limited space available for the movement of mechanism's links. It is not possible for this exoskeleton to raise user's upper arm above the horizontal plane as this will cause part of the 3R mechanism to collide with user's head. This problem is illustrated in Fig. 3.

In order to minimize the negative effects of singular configurations on shoulder movements, some exoskeletons have been designed so that the singular configurations of the 3R mechanism occur at postures that are less likely to interfere with performing rehabilitation exercises.[1–4] This is done by moving the base joint of the 3R mechanism laterally, often by 45° . However, even if the exoskeleton

* Corresponding author. E-mail: hlo015@aucklanduni.ac.nz

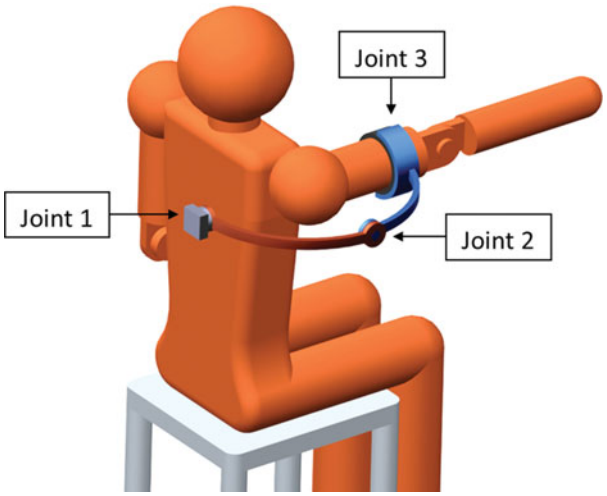

Fig. 1. (Colour online) A 3R exoskeleton in a singular configuration where Joint 3 aligns with Joint 1. In this configuration, the exoskeleton cannot produce horizontal flexion and extension movements of the shoulder.

does not operate exactly at the singular configuration, it will still experience a decrease in performance when it operates nearby.

To demonstrate this, the joint trajectories of the 3R mechanism moving near a singular configuration are shown in Figs. 4 and 5. The movement involves a constant velocity 180° shoulder flexion over 3.5 s in the vertical plane with a 35° medial offset. Since the singular configuration of the 3R mechanism occurs 45° medially from the anterior direction, the 35° medial offset in flexion means the closest the mechanism will operate to the singular configuration is 10° , which occurs when the upper arm is in the horizontal position. At this position, the peak 3R joint velocity occurs at Joint 1 at a very high movement of 296° /s. That is, Joint 1 of the 3R mechanism is required to move at 296° /s to achieve a 51.4° /s shoulder flexion when passing the horizontal upper arm position. Such a high joint velocity is undesirable because first it makes the exoskeleton more dangerous and intimidating to user, and second, it is difficult to achieve such high velocities and accelerations in practice. Movements closer to the singular configuration will require even higher joint velocities.

The 3R mechanism with a 45° offset of the base joint can achieve a larger range of motion than the simpler design in Fig. 3, as it is possible to raise user's arm above the horizontal plane. However, the 3R mechanism will still move dangerously close to user's head (Fig. 6). In addition, raising the upper arm toward the side will require the arm to move close to the base joint of 3R mechanism (Fig. 7).

It is possible to avoid singular configurations and keep the mechanism away from potential collisions if a redundant joint is introduced in the 3R mechanism. The resulting 4-revolute (4R) spherical wrist mechanism (Fig. 8) has one redundant joint, which can be used to keep the system away from singular configurations.[8]

The goal of this paper is to optimize the 4R spherical wrist mechanism for a shoulder exoskeleton and analyze its performance. This paper is organized as follows. The kinematics of the 4R mechanism is presented in Section 2. The optimization problem is outlined in Section 3. Workspace considerations are discussed in Section 4. Singularity analysis is presented in Section 5. An analysis of optimized 4R mechanism is performed in Section 6. Finally, conclusions are presented in Section 7.

2. The 4R Mechanism

The 4R exoskeleton has four revolute joints and is therefore a 4-DOF robot. However, the 4R mechanism is only capable of moving the end-effector in 3 DOF of spherical motion about the instantaneous center of rotation (ICOR). Hence, the 4R exoskeleton can be described as a 4-DOF redundant robot with 3-DOF spherical motion. This redundancy is required to avoid singular configurations of the mechanism and prevent interference with the user while achieving the entire shoulder workspace.

https://doi.org/10.1017/S0263574714001945 Published online by Cambridge University Press

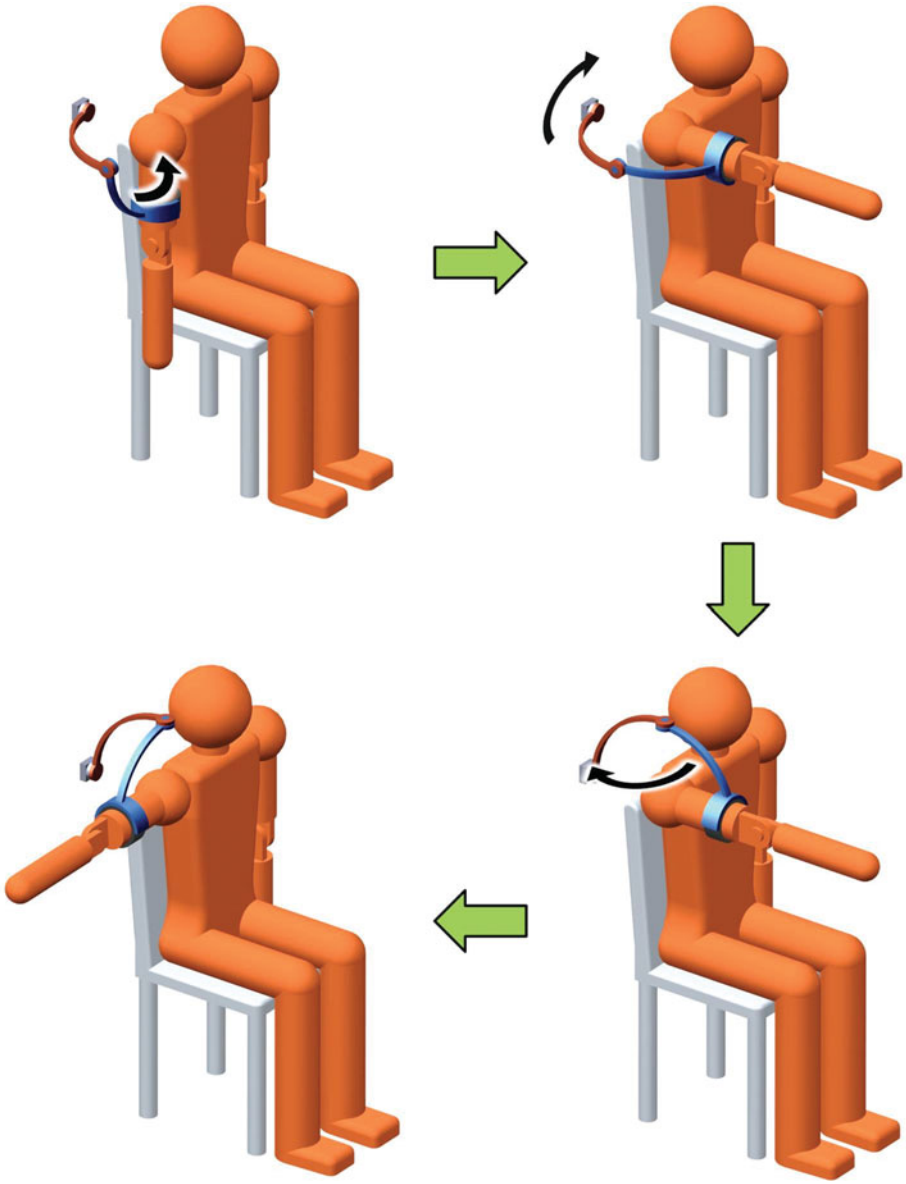

Fig. 2. (Colour online) A 3R exoskeleton moves into a singular configuration shown in the top right where Joint 3 aligns with Joint 1. In this configuration, the exoskeleton cannot produce horizontal flexion and extension of the shoulder unless Joint 1 is repositioned.

The fundamental 4R mechanism consists of a stationary base, an end-effector, and three links (L_1, L_2, L_3) connected in series through four revolute joints (θ_1, θ_2, θ_3, θ_4; Fig. 9). Each of the four revolute joints has an axis of rotation that intersects with the ICOR. The joints are positioned at a suitable distance away from the ICOR so that they do not collide with user's body. This allows the 4R mechanism to operate alongside the human upper arm and mimic the spherical movements of the human shoulder joint. Due to the characteristics of the exoskeleton design, the position and orientation of the robot end-effector directly reflects the posture of user's upper arm. The following terms are used to describe the various aspects of this mechanism:

1. *ICOR*: The center of spherical rotation. All joints of the 4R mechanism intersect at this point. The ICOR of 4R coincides with the ICOR of the human shoulder joint.
2. *Link angle* (α): The angle between two joints in the arc-shaped link about the ICOR.
3. *Joint angle* (θ): The angle of rotational displacement of revolute joint from default position.

https://doi.org/10.1017/S0263574714001945 Published online by Cambridge University Press

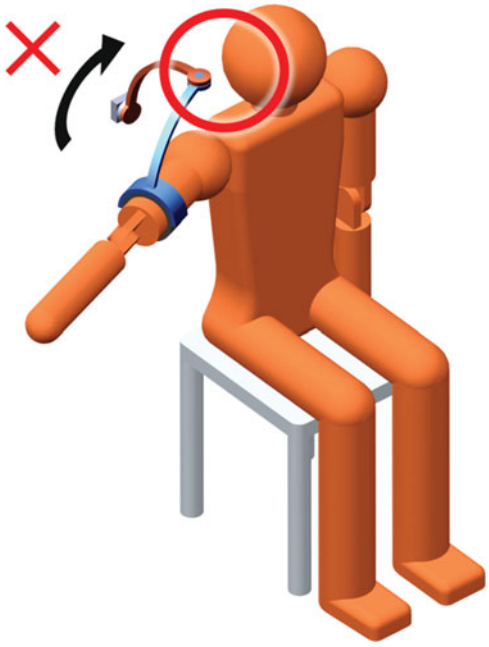

Fig. 3. (Colour online) A 3R exoskeleton with the base joint behind the shoulder cannot raise the upper arm above the horizontal plane as this will cause the mechanism to collide with user's head.

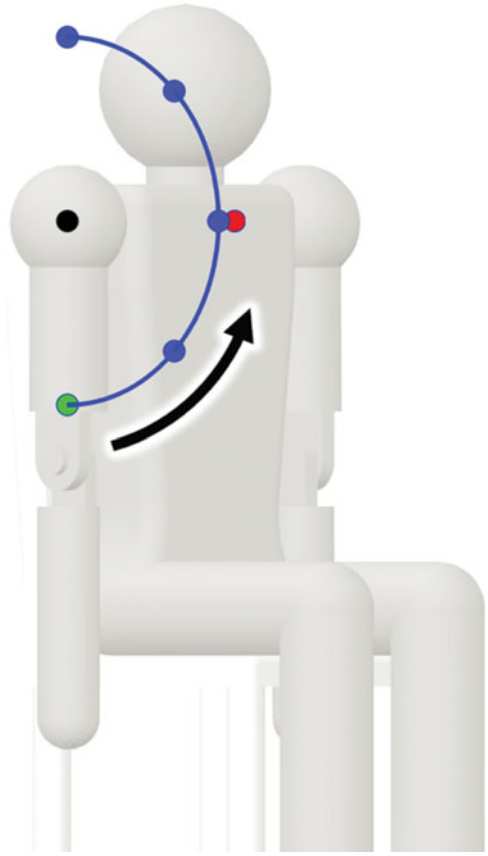

Fig. 4. (Colour online) A trajectory path for 3R mechanism which passes near a singular configuration. This movement is a constant velocity 180° shoulder flexion over 3.5 s along the vertical plane with a 35° medial offset. The green point indicates the starting position of the upper arm and 3R end-effector, and the blue points indicate fixed time steps during the trajectory. The red point represents the position at which a singular configuration of 3R mechanism occurs.

https://doi.org/10.1017/S0263574714001945 Published online by Cambridge University Press

Table I. The DH parameters of a 4R robot.

Link i	a_i	α_i	d_i	θ_i
1	0	α_1	0	θ_1
2	0	α_2	0	θ_2
3	0	α_3	0	θ_3
4	0	0	0	θ_4

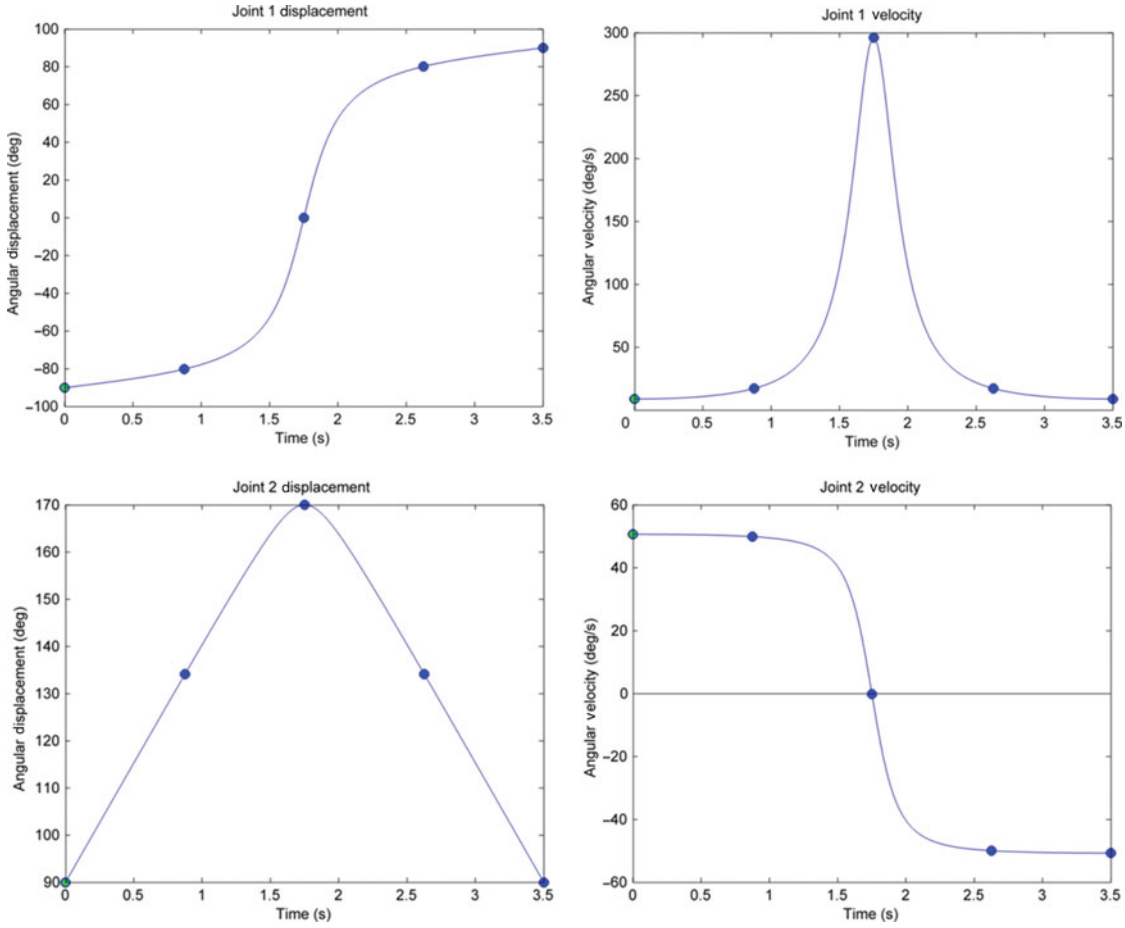

Fig. 5. (Colour online) Position and velocity trajectories of Joints 1 and 2 in 3R mechanism during the 3.5-s shoulder flexion illustrated in Fig. 4.

4. *Joint/end-effector position*: The location of joint/end-effector with respect to ICOR.
5. *Joint configuration*: A combination of joint positions that achieves a certain end-effector position.

The kinematics of a multilink 4R robot is modeled using the Denavit–Hartenberg (DH) notation.[9] The world coordinate system is located at the ICOR with the x-axis pointing to the right, y-axis pointing forward, and z-axis pointing upward with respect to the user as shown in Fig. 12. A coordinate system is defined for each subsequent joint using the DH notation. For simplicity, the coordinate system of each joint is defined with an origin at the ICOR of 4R mechanism, i.e. the length parameters a_i and d_i for all i are zero. This is acceptable because the axis of rotation of all joints in the 4R mechanism always intersect at ICOR. As a result, the occurrence of singular configurations is dependent only on the orientation of joints and independent of the distance between the joints and the ICOR. The DH parameters for a 4R robot are shown in Table I.

https://doi.org/10.1017/S0263574714001945 Published online by Cambridge University Press

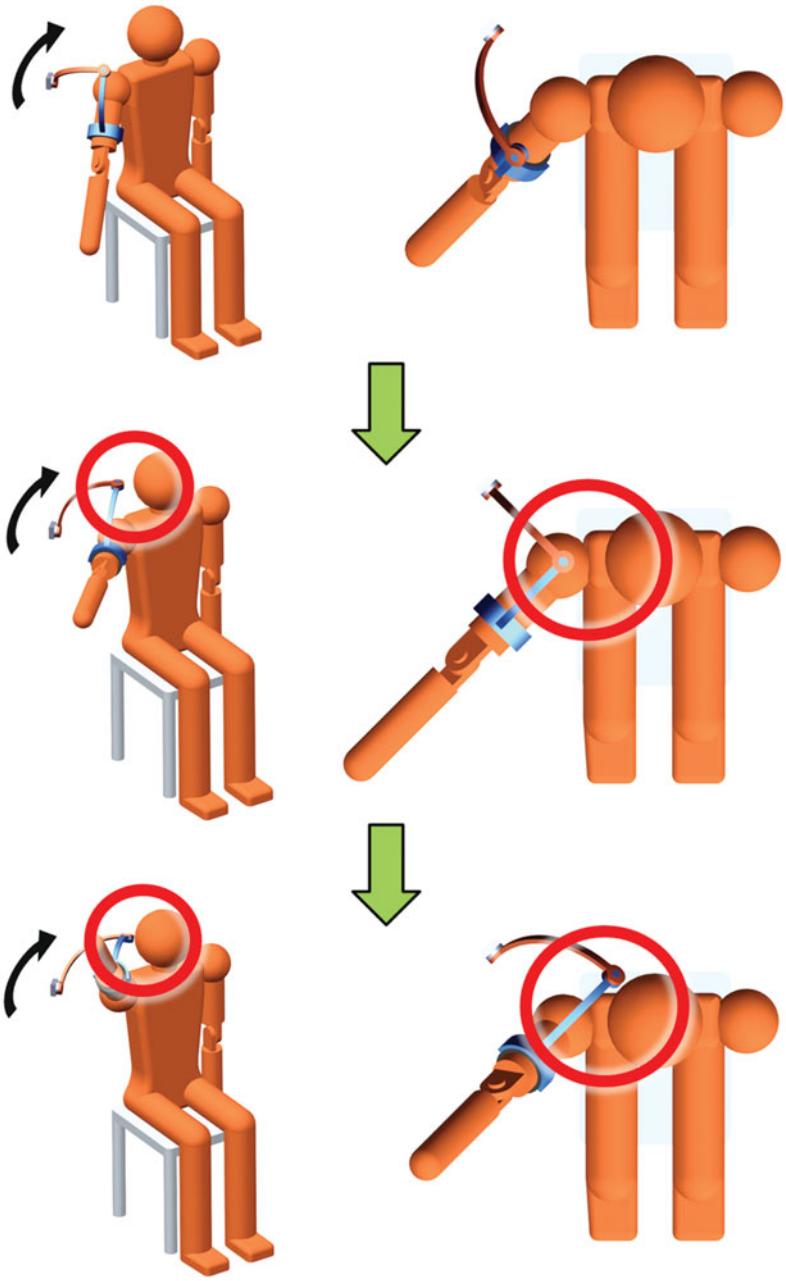

Fig. 6. (Colour online) A 3R exoskeleton with the base joint shifted 45° laterally from behind the shoulder will operate dangerously close to user's head when raising the upper arm above the horizontal plane. The images on the right side show the top view of exoskeleton positions shown on the left side.

3. The Optimization Problem

As mentioned in Section 1, a redundant 4R mechanism can avoid the undesirable singular configurations that occur with a 3R mechanism. The goal of this research work is to optimize the design of a 4R mechanism for a shoulder exoskeleton. The optimization ensures that the additional degrees of freedom provided by the redundant joint is efficiently utilized to achieve the optimal performance of 4R mechanism in the shoulder workspace. This involves finding an optimal design and also an optimal set of joint configurations for the mechanism.

The redundant joint in the 4R mechanism allows some flexibility in the 4R linkage design. Whereas a 3R mechanism requires all link angles to be 90° in order to achieve the full spherical workspace, the link angles of the redundant 4R mechanism can have a variety of sizes and still achieve the full

https://doi.org/10.1017/S0263574714001945 Published online by Cambridge University Press

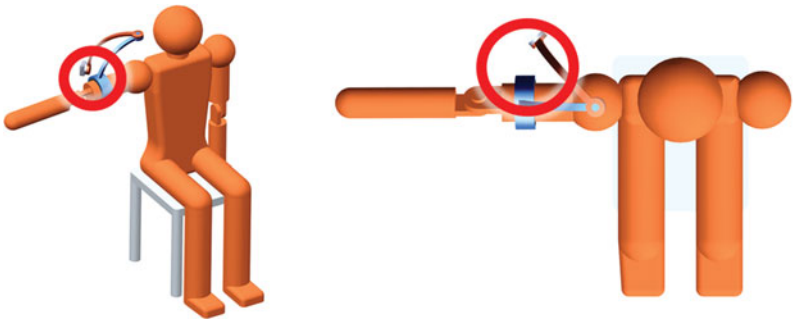

Fig. 7. (Colour online) The upper arm can move dangerously close to the shifted base joint.

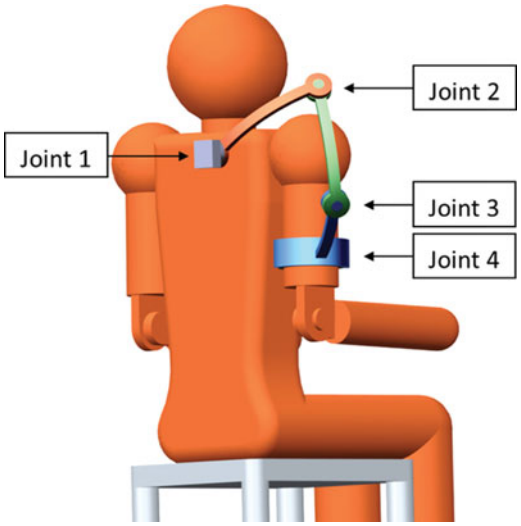

Fig. 8. (Colour online) The 4R exoskeleton concept.

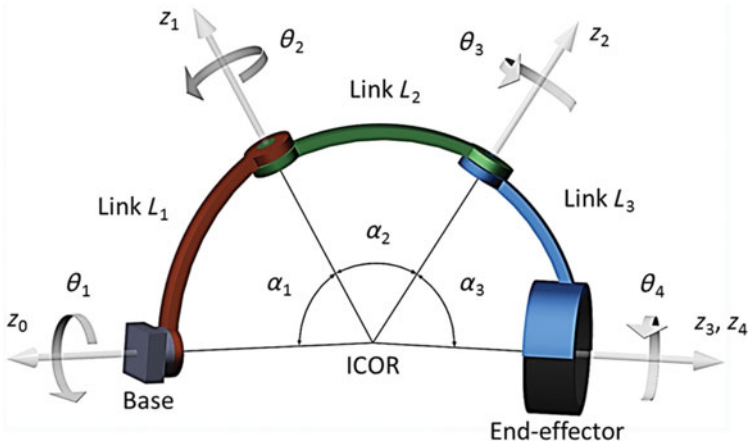

Fig. 9. (Colour online) Parameters of the 4R mechanism.

spherical workspace. Hence, there is a range of possible 4R mechanism designs that can be used in a shoulder exoskeleton. The 4R design can have variations in the sizes of three link angles and the location of the base joint (Fig. 10).

In addition, an issue arising from the redundancy is that it is possible to achieve the same end-effector position with a range of different 4R configurations, i.e. there are infinite inverse kinematics (IK) solutions (Fig. 11). Therefore, it is also necessary to identify the optimal joint configuration for

https://doi.org/10.1017/S0263574714001945 Published online by Cambridge University Press

Table II. Optimization variables.

Variable	Description	Permitted range
α_1	Angle size of L_1	20° to 160°
α_2	Angle size of L_2	20° to 160°
α_3	Angle size of L_3	20° to 160°
φ_z	Spherical coordinate of Joint 1 position about z-axis	−45° to 45°
φ_x	Spherical coordinate of Joint 1 position about x-axis	−90° to 90°
θ_1^0	Joint 1 angle when the end-effector is at the workspace center	−180° to 180°

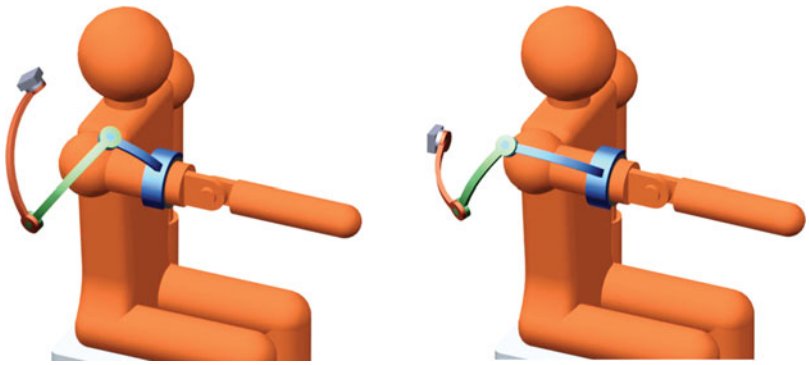

Fig. 10. (Colour online) Example of two different 4R designs with different link angle sizes and base joint position.

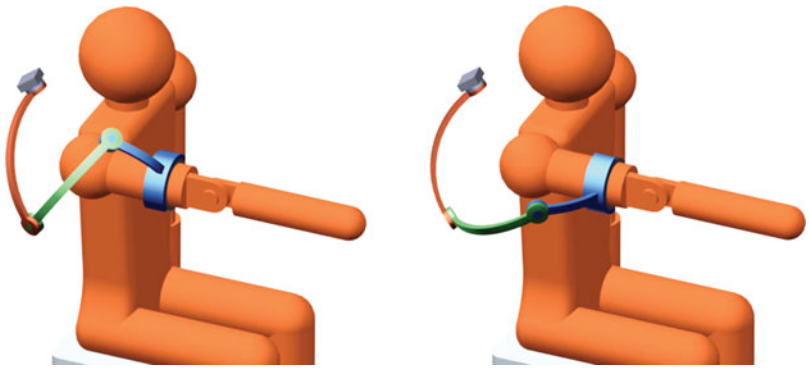

Fig. 11. (Colour online) Example of two different joint configurations of the same 4R design which achieve the same end-effector position.

any given end-effector position in the shoulder workspace. Genetic algorithm is used to solve this complex optimization problem.

3.1. Variables

Six variables are used in this optimization problem. Descriptions of these variables and their permitted values are shown in Table II. The first five variables describe the design of the 4R mechanism, where α_1, α_2, and α_3 describe the three link angles, and φ_z and φ_x describe the position of base joint relative to user's shoulder in spherical coordinates. Here, φ_z precedes φ_x in the sequence of Euler rotations and the default position is directly above the user's shoulder (Fig. 12). The sixth variable θ_1^0 is used to determine the optimal joint configurations of 4R mechanism. This variable is the angle of Joint 1 (θ_1) when the end-effector is at the center of the shoulder workspace. A given value of θ_1 is necessary because there are infinite possible joint configurations for achieving a given end-effector position due to kinematic redundancy. If θ_1 is known, then the angular positions of remaining joints required to achieve the given end-effector position can be determined from IK. However, this only gives the configuration for reaching one position in the workspace. Therefore, an expanding algorithm has

https://doi.org/10.1017/S0263574714001945 Published online by Cambridge University Press

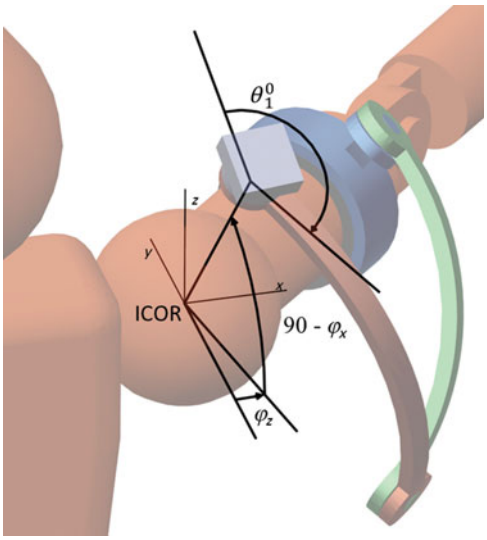

Fig. 12. (Colour online) Illustration of the three positional optimization variables.

been developed to compute joint configurations for reaching the remaining workspace. Further details on this expanding algorithm are provided in Section 4.4. The genetic algorithm generates random solutions, each with a value for six variables within their permitted ranges. Each generation of the algorithm improves these solutions until a set of optimal solutions are obtained.

3.2. Objectives

In this optimization problem, achieving the entire human shoulder workspace is considered to be a compulsory objective. The other performance objectives are average joint transition, global condition number, and maximum condition number. The genetic algorithm uses these objectives to evaluate the performance of each solution and the best performing solutions are selected for producing the next generation of solutions. These objectives are discussed in the subsequent sections.

4. Workspace of the 4R Mechanism

The 4R mechanism is intended for a shoulder exoskeleton, therefore the workspace of the human shoulder needs to be considered in the design. The workspace for the human shoulder is approximately half of the spherical workspace, while the 4R exoskeleton can be designed to operate the end-effector in the entire spherical workspace. Since the exoskeleton is only required to operate in the shoulder workspace, compromises can be made in the 4R design to sacrifice performance in the workspace that the human shoulder cannot reach to improve performance in the workspace which the shoulder can reach. Hence, the 4R design is optimized only for the shoulder workspace rather than the entire spherical workspace. However, it is difficult to find all the optimal joint configurations for the entire continuous workspace of this non-linear system. Therefore, optimal configurations will be determined for a pre-defined set of end-effector positions in the shoulder workspace.

4.1. Workspace discretization

The shoulder workspace is discretized into points, each indicating an end-effector position to be analyzed. For each end-effector position, a 4R mechanism configuration with good performance will be identified. A common method for allocating points on the surface of a sphere is by using the longitude and latitude parameters. However, this method results in a non-uniform distribution of points with a higher density of points at the two poles of the sphere. This causes the performance near the poles to have a larger influence on the overall performance score. Ideally the points should be uniformly distributed to ensure that the workspace is analyzed evenly.

A set of 89 uniformly distributed points over the shoulder workspace are generated using an algorithm that performs repeated subdivisions of a spherical icosahedron to obtain a grid of evenly distributed points on the surface of a sphere.[10] The number of uniformly distributed points N that

https://doi.org/10.1017/S0263574714001945 Published online by Cambridge University Press

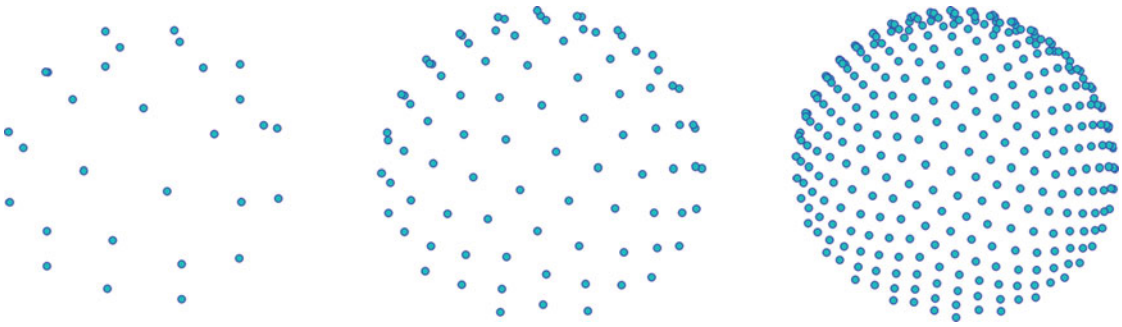

Fig. 13. (Colour online) Uniformly distributed semi-sphere points obtained from spheres with 42, 162, and 642 points respectively.

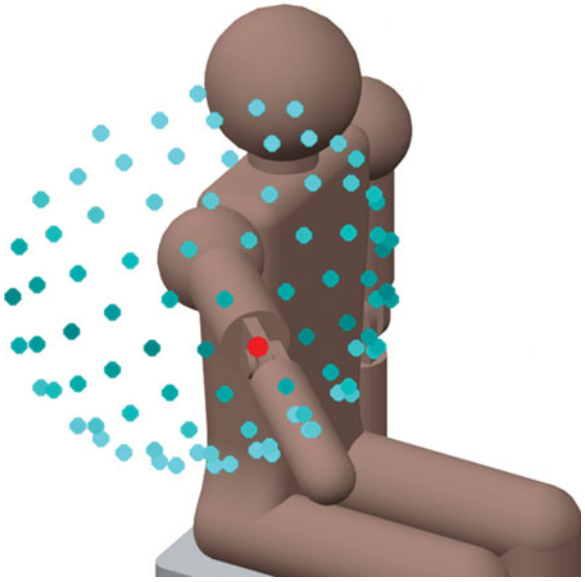

Fig. 14. (Colour online) Eighty-nine uniformly distributed points are used to analyze the shoulder workspace. The model user shown has a shoulder posture at the center of the workspace, represented by a red point.

can be obtained using this algorithm is calculated using the following equation:

$$N = 2 + \left(10 \times 4^{k}\right)', \tag{1}$$

where k is a positive integer.

The four lowest number of uniform spherical points that can be obtained from this method are 12, 42, 162, and 642 points. Fig. 13 shows the semi-spheres for the three latter cases. A sphere of 162 points is selected for representing the end-effector positions as this has a sufficient point density to provide a good representation of 4R performance over the workspace. Since only the shoulder workspace is required rather than the entire spherical workspace, only 89 of the 162 points are used. These points cover a semi-spherical region in the lateral-anterior region of user's shoulder (Fig. 14). The optimal joint configurations to reach each of the 89 end-effector positions are determined using the expanding algorithm in Section 4.4. Interpolation can then be used to find joint configuration to reach any arbitrary end-effector position in the shoulder workspace.

4.2. Workspace limitations

As mentioned in Section 3.2, achieving the entire shoulder workspace is a compulsory objective of 4R mechanism. The workspace of 4R mechanism is limited by three factors. If any of these three factors occur for a given joint configuration, the end-effector position under consideration is classified as unreachable. The first case occurs when there is no IK solution for the given end-effector position

https://doi.org/10.1017/S0263574714001945 Published online by Cambridge University Press

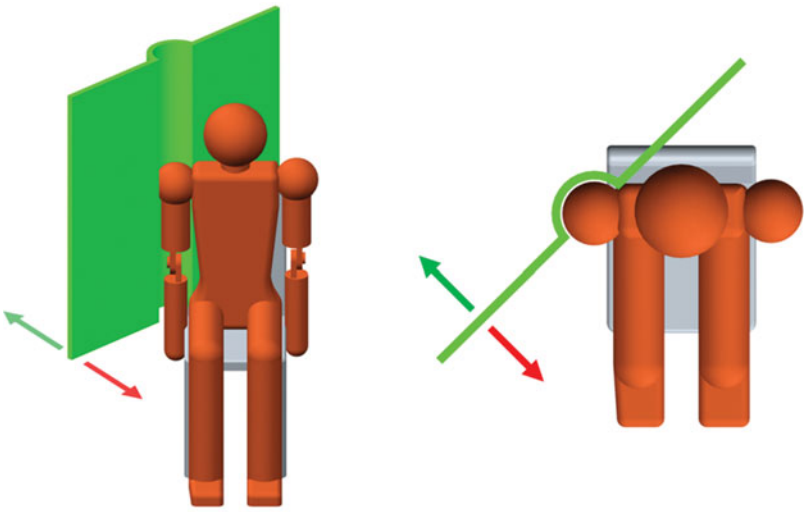

Fig. 15. (Colour online) Boundary of a forbidden region for the mechanism structure. The red arrow indicates the region that is forbidden and the green arrow indicates the permitted operating region.

and Joint 1 angle. The method used to identify this situation is explained in Section 4.3. The second case occurs when the joint configuration is at or very close to a singular configuration. Since there are significant limitations in operating at a singular configuration, the end-effector position that causes the singular configuration cannot be included in the operating workspace. Singularity analysis is discussed in Section 5.

The final case occurs when a part of 4R mechanism is required to enter a forbidden region to reach an end-effector position. These include regions that can harm or cause discomfort for the user. The robot can harm the user if the robot links collide with a part of user's body. With the design concept used, the robot links can potentially collide with user's torso, neck, or head when moving toward a certain end-effector position. Therefore, the links must not enter user's medial region with respect to ICOR. Furthermore, operating the links in user's field of view can cause uneasiness and discomfort for the user. Therefore, the links must also not enter user's anterior region. Joint configurations that require the links to enter user's medial or anterior regions are not permitted and are classified as unreachable. The boundary for this region is specified by a vertical plane intersecting the ICOR with a normal axis in the anterior-medial direction, 45° from the anterior axis. In addition, regions near the head and torso are also forbidden, i.e. regions above and below the ICOR. This region is represented by a vertical cylindrical volume with an axis intersecting the ICOR. The boundary is shown in Fig. 15.

4.3. Inverse kinematics

There are infinite solutions to the IK problem for any given end-effector position due to the redundancy of 4R mechanism. However, if the desired end-effector position and the joint angle of one of the three proximal joints are known, then the angles of the remaining joints can be derived using IK. In this work, θ_1 is generated by the algorithm. Therefore, the IK problem now involves finding the configuration of a non-redundant 3R mechanism, i.e. the angular positions θ_2, θ_3, and θ_4. However, θ_4 only affects the axial orientation of the end-effector and not the position since the end-effector is located in the same position as Joint 4. Hence, the end-effector position (i.e. shoulder flexion and extension, and abduction and adduction) is dependent on θ_1, θ_2, and θ_3, while the end-effector axial orientation (i.e. shoulder medial and lateral rotation) is dependent on θ_4. The resulting IK problem is then to find θ_2 and θ_3 to achieve the desired end-effector position with a given value of θ_1. Essentially, the positions of Joints 1, 2, and 4 are known and the position of Joint 3 needs to be found.

The IK problem for a 4R robot is solved using a heuristic iterative method based on the Forward and Backward Reaching Inverse Kinematics (FABRIK) algorithm.[11] An iteration of the FABRIK method is a two-stage process that begins at the last joint in the chain and works inwards, adjusting the position of each joint along the way. This process is then repeated outwards in the second stage to

https://doi.org/10.1017/S0263574714001945 Published online by Cambridge University Press

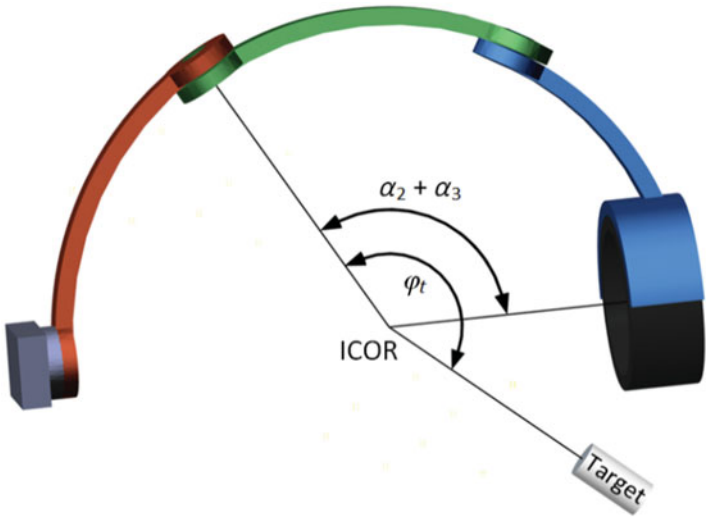

Fig. 16. (Colour online) Example of the first condition for unreachable target (Eq. (2a)).

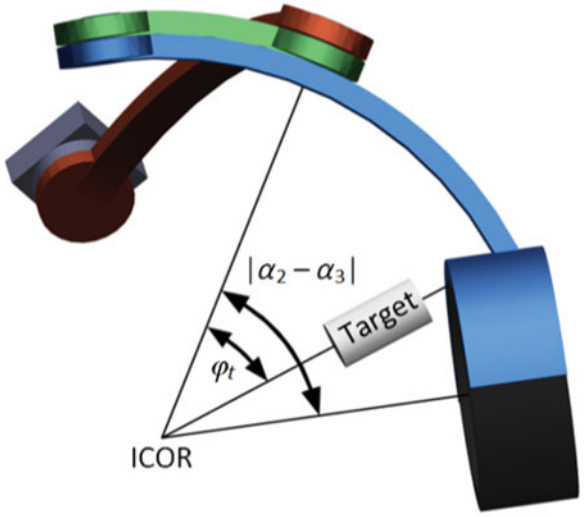

Fig. 17. (Colour online) Example of the second condition for unreachable target (Eq. (2b)).

complete a full iteration. Each iteration moves the end-effector closer to the target position. Hence, iterations are repeated until the end-effector is sufficiently close to the specified target position.

First, the conditions that cause a target end-effector position to be unreachable by the 4R mechanism are identified since there will not be an IK solution. The end-effector of 4R cannot reach a target position if any of the following geometric conditions are met. These are when the angle at the ICOR between Joint 2 and the target end-effector position φ_t is greater than the sum of the link angles α_2 and α_3 (Fig. 16), or smaller than the difference between the link angles α_2 and α_3 (Fig. 17), i.e. the target is unreachable if:

$$\varphi_t > \alpha_2 + \alpha_3, \tag{2a}$$

$$\varphi_t < |\alpha_2 - \alpha_3|\,. \tag{2a}$$

These conditions apply to the problem specified at the beginning of this section, in which the positions of Joints 1 and 2 and target position of Joint 4 are known and the position of Joint 3 required to achieve the specified position of Joint 4 needs to be determined. In addition, distal joints are not permitted to be positioned under a proximal link. This is to ensure that the links will not collide with actuators attached to the joints. The FABRIK algorithm is terminated once a configuration is obtained

https://doi.org/10.1017/S0263574714001945 Published online by Cambridge University Press

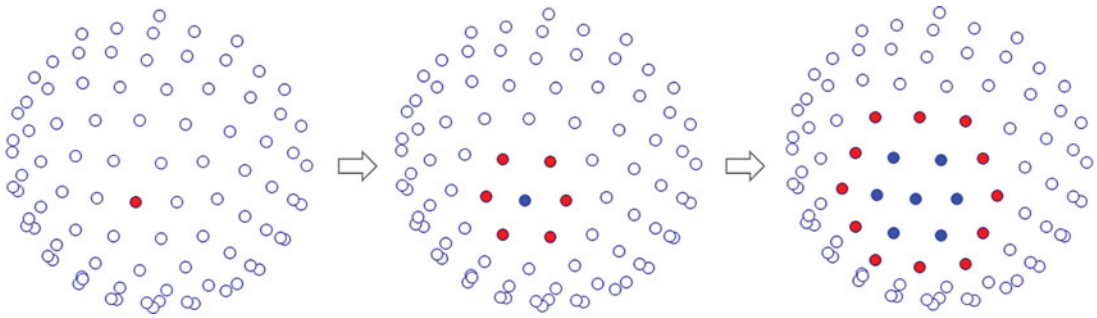

Fig. 18. (Colour online) The first two iterations in the expanding algorithm. Each iteration finds joint configurations for a new layer of end-effector positions. The red points represent the positions to be analyzed in the current iteration, and the blue points represent the positions that have already been analyzed in a previous iteration.

with an end-effector position error of less than 1° . This configuration is selected as a solution to the IK problem. In addition, the algorithm is terminated if the error threshold is not achieved after 2,000 iterations as a precaution to prevent infinite loops. This threshold was not reached during the optimization process.

4.4. Optimization for the entire workspace

The IK discussed in Section 4.3 only computes the joint configuration for one end-effector position in the shoulder workspace. An optimal joint configuration needs to be found for each of the 89 end-effector positions. However, if an optimal joint configuration is found for each end-effector position independently, then the end-effector positions that are adjacent to one another may have very different joint configurations, and therefore require large joint movements. Ideally, the optimal joint configuration identified for every end-effector position will be able to transition to an adjacent position smoothly with minimal joint displacements. This is a part of the average joint transition objective defined in the optimization problem. An expanding algorithm has been developed to obtain optimal joint configurations for all 89 end-effector positions in the shoulder workspace. This makes use of the value θ_1^0 generated by the genetic algorithm as the sixth variable. This variable is the value of θ_1 for reaching the end-effector position at the center of the shoulder workspace.

The expanding algorithm first finds the optimal joint configuration for this center position using workspace and singularity analysis with the six variable values provided by the genetic algorithm. The algorithm then computes optimal joint configurations for all end-effector positions adjacent to this starting position. This is done while ensuring that the transition between adjacent end-effector positions is realistic, requires minimal joint displacements, causes minimal interference with the user, and avoids approaching a singular configuration. This is achieved by generating a range of θ_1 values for the adjacent child position, which are within 20° of the parent positions' θ_1 value, and analyzing the performance of their respective joint configurations. The θ_1 value that gives the best performing joint configuration is then selected as the optimal for the child end-effector position. This is done for each end-effector position that is adjacent to the parent position and has not already been analyzed. The process is then applied to the next layer of adjacent end-effector positions and repeated until all 89 positions in the shoulder workspace have been investigated (Fig. 18).

By starting from the center end-effector position in the workspace, the expanding algorithm is completed with the minimum number of iterations. The overall ease of transition between every combination of adjacent end-effector positions is used as part of the average joint transition objective in the genetic algorithm optimization. This is calculated as an average change in joint angles of the three proximal joints in the 4R mechanism between the joint configurations of every pair of adjacent end-effector positions. The objective is to minimize this value. The resulting set of 89 θ_1 values, which achieves optimal joint configurations for reaching the 89 end-effector positions, will be used to control the redundant robot. Interpolation of 89 configurations can be done to find joint configuration for any arbitrary end-effector position in the shoulder workspace.

4.5. Shoulder axial rotation

Joint 4 in 4R mechanism can independently adjust shoulder axial rotation due to its kinematic structure. This joint is implemented using an arc-shaped rail mechanism around the upper arm and

https://doi.org/10.1017/S0263574714001945 Published online by Cambridge University Press

has a size requirement which depends on the range of motion requirement. A small range of motion requirement of Joint 4 is preferable as this means a smaller sized rail can be used, which makes the exoskeleton easier to don and also reduces the amount of interference with the user.

Due to the kinematics of the 4R spherical wrist mechanism, the zero position of Joint 4 shifts as the mechanism configuration changes. This shift is dependent on 4R mechanism's kinematic design. In addition, the range of motion of shoulder axial rotation also changes depending on shoulder's posture. Experiments done by Wang *et al.*[12] show that as the shoulder is horizontally flexed, the limit of medial rotation decreases while the limit of lateral rotation increases. A deviation between two zero positions will require Joint 4 to have a larger range of motion to ensure that exoskeleton can reach the extreme limits of shoulder axial rotation. Therefore, to minimize the range of motion requirement of Joint 4, its zero position needs to be kept close to the zero position of shoulder axial rotation for the entire shoulder workspace. The maximum deviation between the two zero positions in both clockwise and counter-clockwise rotational directions determine the additional range of motion required in Joint 4. The minimization of this deviation is part of the average joint transition objective. In this work, the zero position of shoulder axial rotation is assumed to shift linearly up to 45° between the limits of horizontal flexion and extension.

5. Singularity Analysis

It is desirable to have the robot operate far away from singular configurations in order to reduce joint velocities. Singularity analysis is done using Jacobian matrices and its condition number (CN).[13] The Jacobian matrix of a robot (J) maps robot's joint velocities to the angular velocity of the end-effector:

$$\omega = J\dot{\theta}, \tag{3}$$

where ω is end-effector's angular velocity, J is the Jacobian matrix, and $\dot{\theta}$ is the joint velocity vector.

The Jacobian matrix for a 4R mechanism is a 3×4 non-square matrix due to redundant joint. Each column represents kinematic relationship between end-effector and one of the four revolute joints,

$$\omega = \begin{bmatrix} J_1 & J_2 & J_3 & J_4 \end{bmatrix} \begin{bmatrix} \dot{\theta}_1 \\ \dot{\theta}_2 \\ \dot{\theta}_3 \\ \dot{\theta}_4 \end{bmatrix}, \tag{4}$$

where $J = \begin{bmatrix} J_1 & J_2 & J_3 & J_4 \end{bmatrix}$ and is a 3×4 matrix with J_1, J_2, J_3, and J_4 representing kinematic relationships between the angular velocity of the 4R end-effector ω and the angular rates $\dot{\theta}_1$, $\dot{\theta}_2$, $\dot{\theta}_3$, and $\dot{\theta}_4$ of Joints 1, 2, 3, and 4 respectively.

Due to the spherical nature of 4R mechanism and the assignment of DH coordinate systems at ICOR, the Jacobian for each joint can be obtained from the DH transformation matrix T_4^{i-1} relating the respective joint to end-effector:

$$J_i = \begin{bmatrix} n_z \\ o_z \\ a_z \end{bmatrix}_4^{i-1}, \tag{5}$$

where n_z, o_z, and a_z are obtained from the DH transformation matrix:

$$T_4^{i-1} = \begin{bmatrix} n_x & o_x & a_x & r_x \\ n_y & o_y & a_y & r_y \\ n_z & o_z & a_z & r_z \\ 0 & 0 & 0 & 1 \end{bmatrix}. \tag{6}$$

https://doi.org/10.1017/S0263574714001945 Published online by Cambridge University Press

Table III. 4R variable values of the selected solution.

Design variable	Optimal value (°)
α_1	88.9
α_2	79.9
α_3	62.9
φ_z	9.0
φ_x	35.2
θ_1^0	−149.0

Table IV. Comparison between 4R and 3R designs.

Design	GCN	CN_{max}	Average joint transition
Optimized 4R	1.7	2.4	9.3°
4R with 90° links and base behind ICOR	1.9	5.0	13.9°
3R with base offset by 45°	2.4	8.0	14.3°

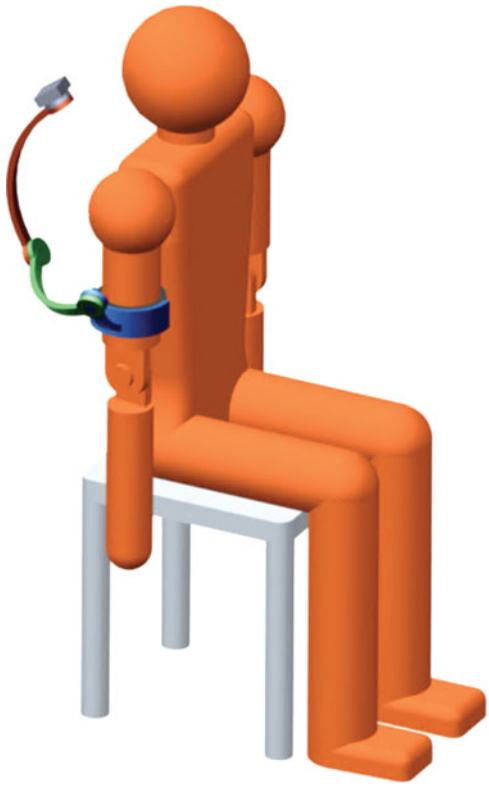

Fig. 19. (Colour online) A 4R mechanism with the optimal parameters given in Table III.

The singular values are defined as the square root of eigenvalues of $\bar{J}J^T$ and $\bar{J}^T\bar{J}$. These singular values are obtained by factorizing J using the singular value decomposition rule:

$$[J]_{4\times3} = \left[X^T\right]_{4\times4}[\Sigma]_{4\times3}[Y]_{3\times3}\,, \tag{7}$$

where X and Y are orthogonal matrices and Σ is a diagonal matrix of three singular values which are related as $\sigma_1 \geq \sigma_2 \geq \sigma_3 \geq 0$.

https://doi.org/10.1017/S0263574714001945 Published online by Cambridge University Press

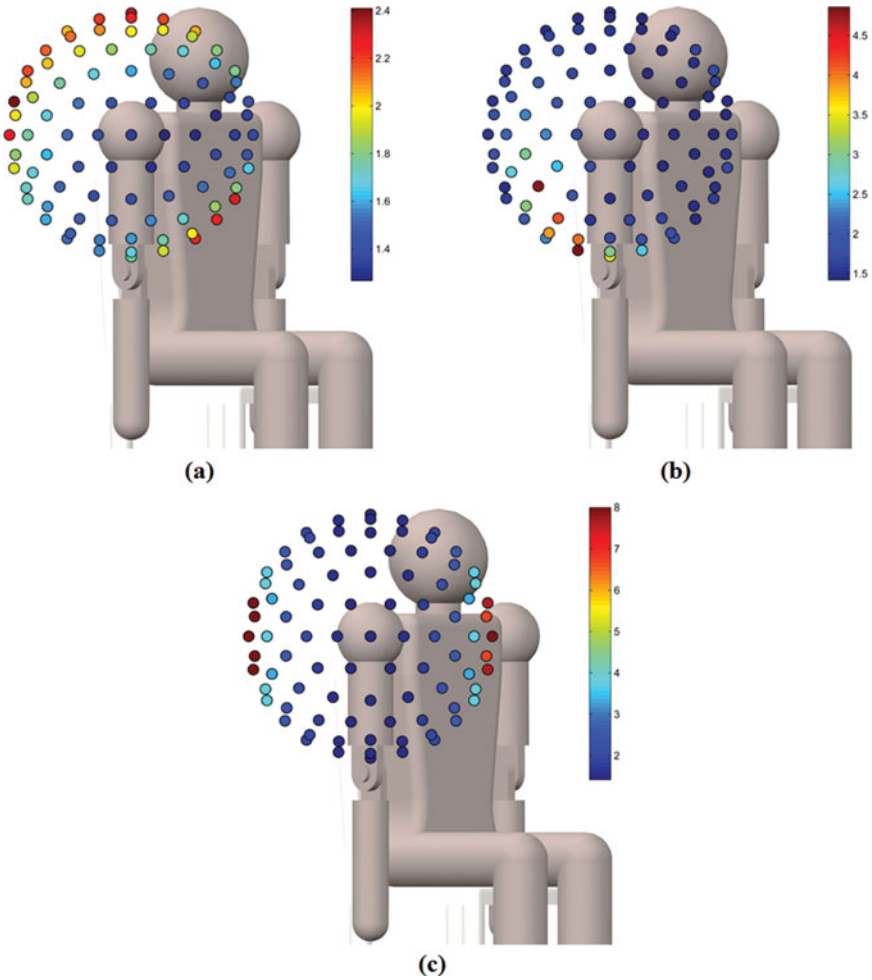

Fig. 20. (Colour online) CN results for the workspace of three different designs: (a) Optimized 4R, (b) 4R with 90° links and base joint behind the shoulder, and (c) 3R with the base joint rotated 45° laterally from behind the shoulder.

The CN of the Jacobian matrix $k(J)$ is then defined as the ratio of the largest singular value σ_1 to the smallest singular value σ_3 :

$$k\left(J\right) = \frac{\sigma_1}{\sigma_3}, \tag{8}$$

where the range of CN is:

$$1 \leq k\left(J\right) \leq \infty. \tag{9}$$

The CN indicates how far away is the specified configuration from the nearest singular configuration. The closer the CN is to unity, the further away is the configuration from a singular configuration. Therefore, the objective is to optimize 4R to operate in configurations with a CN value close to unity. This is a minimization problem.

The CN value is different for different configurations. Therefore, to get a more comprehensive summary of the CN distribution over the shoulder workspace, the global condition number (GCN) is used,

$$\text{GCN} = \frac{\sum_{i=1}^{n}\left(k\left(i\right)\right)}{n} \tag{10}$$

https://doi.org/10.1017/S0263574714001945 Published online by Cambridge University Press

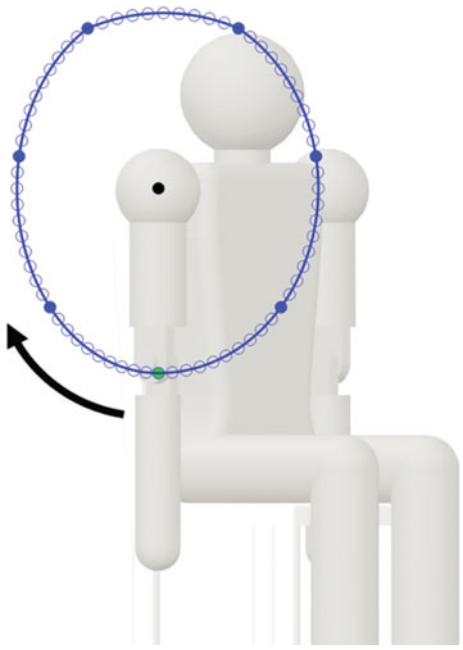

Fig. 21. (Colour online) A trajectory path for the optimized 4R mechanism where it operates closest to singular configurations. This movement is a constant velocity shoulder circumduction over 7 s. Each point indicates a position of the upper arm and 4R end-effector. The green point indicates the starting and ending positions, the solid blue points indicate the positions at every time step of 1 s, and the white points indicate the positions at every time step of 0.1 s.

Here, $n = 89$ and is the total number of workspace positions, and the numerator is the sum of the CN values obtained for each of these positions. However, GCN can overlook the occurrence of undesirable peak CN values. To ensure these peak values are not overlooked, the maximum CN value out of the 89 values calculated for the workspace (CN_{max}) is also considered in the optimization process,

$$CN_{max} = \max\left(k\left(1\right), \ldots, \; k\left(n\right)\right). \tag{11}$$

6. Optimization Results

The design optimization of 4R mechanism was carried out using the variables and objectives discussed in Section 3. The optimization problem was formulated in MATLAB and the genetic algorithm was applied with a crossover probability of 0.9, and a mutation probability of 0.167. A solution with relatively smaller link angles is selected from the set of optimal solutions. The optimal variable values of the selected solution are shown in Table III. A 4R exoskeleton designed with these variable values can theoretically achieve 100% of the shoulder workspace without interfering with the user. Fig. 19 illustrates a 4R exoskeleton with these parameter values.

For comparison, the algorithm is applied to two other designs: a 4R mechanism with 90° link sizes and the base joint behind the shoulder, and a 3R mechanism with the base joint rotated 45° laterally from behind the shoulder. The GCN and the maximum CN values for all three designs are shown in Table IV. However, in analyzing the 3R mechanisms, a workspace constraint that was imposed during the optimization of 4R is removed. This constraint prevented the mechanism links from entering the region above the shoulder and is removed because it significantly reduced the workspace of 3R mechanisms. As a result, the 3R mechanism will operate closer to user's head than the 4R mechanism.

As discussed in Section 5, the robot configuration is further away from a singular configuration if the CN value is closer to unity. The optimized 4R design has both GCN and maximum CN value that is closer to unity compared with other designs. The lower GCN value of 1.7 for the optimized 4R compared with 1.9 for the un-optimized 4R and 2.4 for 3R indicates that on average this 4R exoskeleton is able to operate further from singular configurations than the other designs

https://doi.org/10.1017/S0263574714001945 Published online by Cambridge University Press

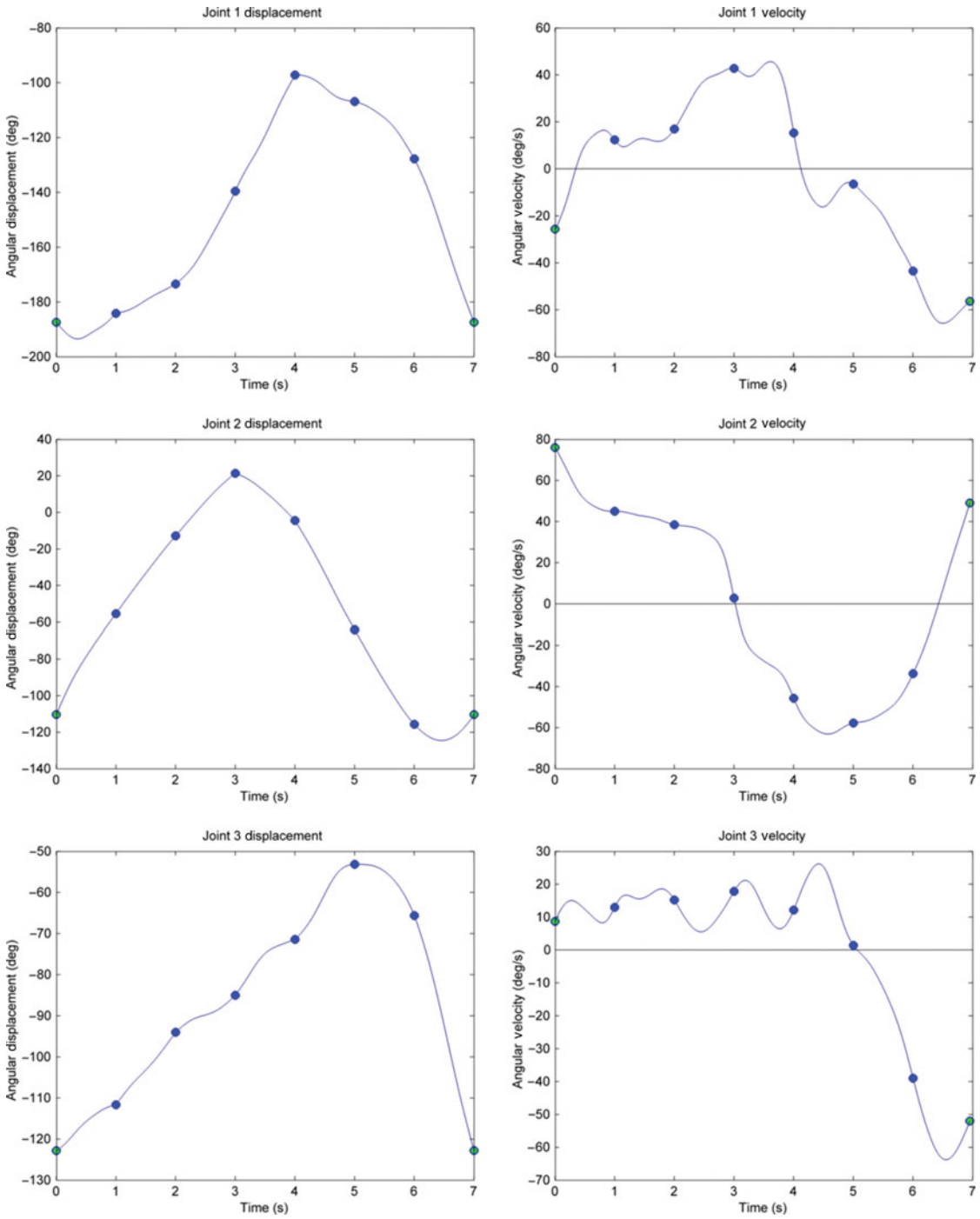

Fig. 22. (Colour online) Position and velocity trajectories of Joints 1, 2, and 3 in the optimized 4R mechanism during the 7-s shoulder circumduction illustrated in Fig. 21.

when operating in the shoulder workspace. A small maximum CN value of 2.4 for the optimized 4R indicates that this design can achieve the entire shoulder workspace with configurations that are all relatively far from a singular configuration. Fig. 20 shows CN values over the shoulder workspace for each design.

The optimized 4R mechanism operates closest to singular configurations when at the edge of the shoulder workspace. An example of the trajectories of Joints 1, 2, and 3 in performing a circular movement of the upper arm along the edge of the workspace is presented in Figs. 21 and 22. This circumduction movement involves approximately 360° rotation of the shoulder and is done with a

https://doi.org/10.1017/S0263574714001945 Published online by Cambridge University Press

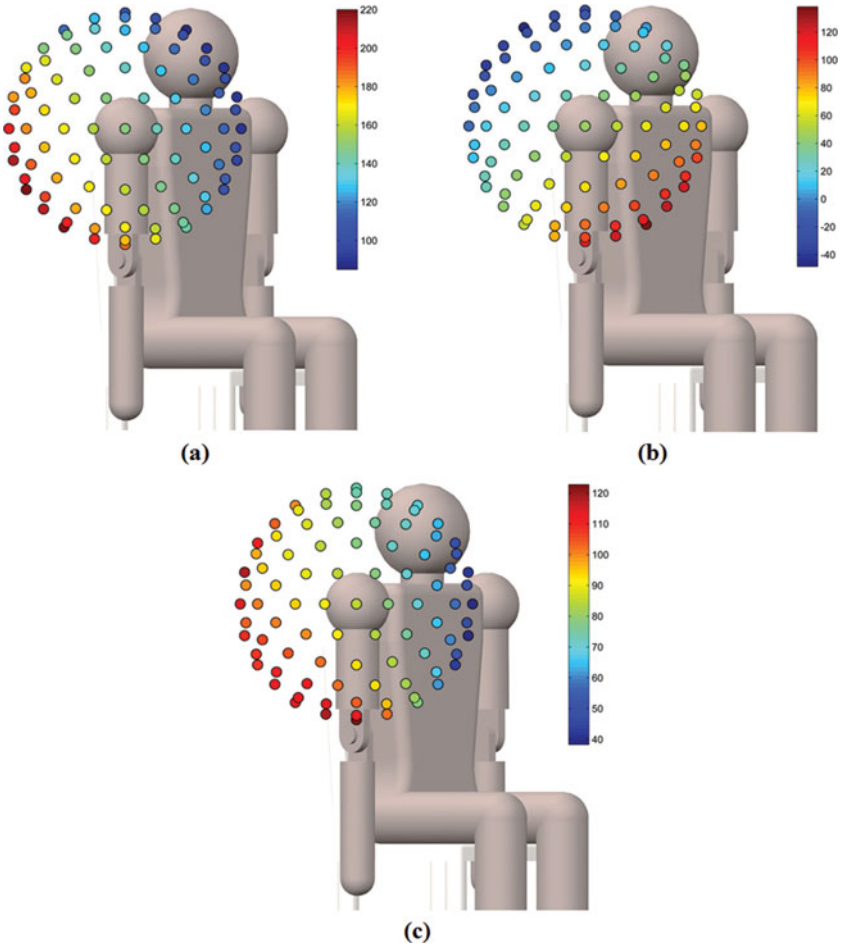

Fig. 23. (Colour online) Displacement angles of Joints 1, 2, and 3 to optimally reach each of the 89 end-effector positions. (a) Joint 1 angles. (b) Joint 2 angles. (c) Joint 3 angles.

near-constant velocity of 51.4° /s over 7 s. The peak 4R joint velocity during this movement occurs at Joint 2 at 76° /s. Joints 1 and 3 have slightly lower peak velocities at 65° /s and 63° /s respectively. These joint velocities are at comfortable and feasible levels, which are close to that of the shoulder joint itself. In contrast, example in Section 1 of a 3R mechanism passing near a singular configuration had a peak joint velocity of 296° /s.

Furthermore, the optimized 4R design has a lower average joint transition angle of 9.3° compared with 13.9° for the un-optimized 4R and 14.3° for 3R designs. This implies that the joints of the optimized 4R move at a lower velocity when moving the end-effector through the shoulder workspace compared with other designs.

Figure 23 shows the optimal joint angles of Joints 1, 2, and 3 to reach each of the 89 end-effector positions in the shoulder workspace. These joint angles combine to give optimal joint configurations selected by the optimization algorithm for the optimized 4R mechanism. It can be seen in Fig. 23 that each joint can smoothly transition between adjacent end-effector positions in all directions without requiring sudden changes in joint angle. Fig. 24 shows that the offset between the zero positions of Joint 4 and that of shoulder axial rotation is minimal for the majority of workspace. The larger offset occurs at the workspace boundary in the horizontally extended position. These boundary positions are difficult to reach for a typical shoulder and should not be an issue. A small offset means that Joint 4 can be implemented using a small arc-shaped rail with an arc size similar to the range of motion of shoulder axial rotation. A small rail makes the exoskeleton easier for the user to don and does not have the problem that a 360° circular rail has, where the rail collides with the user's torso when the upper arm is lowered.

https://doi.org/10.1017/S0263574714001945 Published online by Cambridge University Press

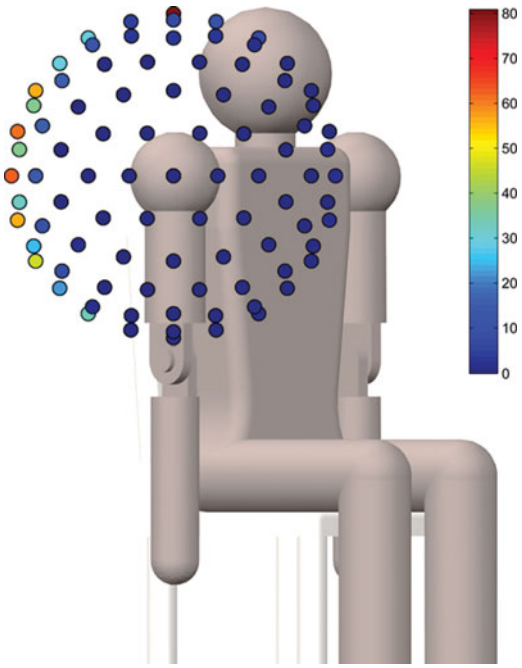

Fig. 24. (Colour online) Angular offset between the zero position of Joint 4 and the zero position of shoulder axial rotation when using the optimal joint positions shown in Fig. 23.

7. Conclusions

This paper presented the design of a redundant 4R spherical wrist mechanism for a shoulder exoskeleton to solve the singularity problem present in the popular 3R spherical wrist. The 4R mechanism has been optimized using genetic algorithm to achieve the entire human shoulder workspace while operating far away from singular configurations and without interfering with the user. The optimization process has acquired an optimal 4R mechanism design as well as a set of optimal joint configurations for reaching 89 positions in the shoulder workspace. Analysis of these configurations confirms feasible and smooth movements of each joint in the 4R mechanism throughout the shoulder workspace.

References

1. J. C. Perry, J. Rosen and S. Burns, "Upper-limb powered exoskeleton design," *IEEE/ASME Trans. Mechatronics* **12**(4), pp. 408–417 (2007).
2. D. Naidu, R. Stopforth, G. Bright and S. Davrajh, "A 7-DOF exoskeleton arm: Shoulder, elbow, wrist and hand mechanism for assistance to upper limb disabled individuals," *IEEE AFRICON Conference*, Livingstone, Zambia (Sep. 13–15, 2011).
3. C. Carignan, J. Tang and S. Roderick, "Development of an exoskeleton haptic interface for virtual task training," **In**: *IEEE/RSJ International Conference on Intelligent Robots and Systems*, St. Louis, USA (Oct. 11–15, 2009) pp. 3697–3702.
4. S. J. Ball, I. E. Brown and S. H. Scott, "MEDARM: A rehabilitation robot with 5-DOF at the shoulder complex," *IEEE/ASME International Conference on Advanced Intelligent Mechatronics*, Zurich, Switzerland (Sep. 4–7, 2007).
5. F. Martinez, A. Pujana-Arrese, I. Retolaza, I. Sacristan, J. Basurko and J. Landaluze, "IKO: A five actuated DoF upper limb exoskeleton oriented to workplace assistance," *Appl. Bionics Biomech.* **6**(2), pp. 143–155 (2009).
6. T. Nef, M. Guidali and R. Riener, "ARMin III – Arm therapy exoskeleton with an ergonomic shoulder actuation," *Appl. Bionics Biomech.* **6**(2), pp. 127–142 (2009).
7. H. S. Lo and S. Q. Xie, "Exoskeleton robots for upper-limb rehabilitation: State of the art and future prospects," *Med. Eng. Phys.* **34**(3), pp. 261–268 (2012).
8. H. S. Lo and S. S. Q. Xie, "Optimization of a redundant 4R robot for a shoulder exoskeleton," **In**: *IEEE/ASME International Conference on Advanced Intelligent Mechatronics*, Wollongong, Australia (Jul. 9–12, 2013) pp. 798–803.

https://doi.org/10.1017/S0263574714001945 Published online by Cambridge University Press

9. J. Denavit and R. S. Hartenberg, "A kinematic notation for lower pair mechanisms based on matrices," *ASME J. Appl. Mech.* **23**, 215–221 (1955).
10. N. A. Teanby, "An icosahedron-based method for even binning of globally distributed remote sensing data," *Comput. Geosci.* **32**(9), 1442–1450 (2006).
11. A. Aristidou and J. Lasenby, "FABRIK: A fast, iterative solver for the inverse kinematics problem," *Graph. Models* **73**(5), 243–260 (2011).
12. X. Wang, M. Maurin, F. Mazet, N. D. C. Maia, K. Voinot, J. P. Verriest and M. Fayet, "Three-dimensional modelling of the motion range of axial rotation of the upper arm," *J. Biomech.* **31**(10), 899–908 (1998).
13. P. K. Jamwal, S. Xie and K. C. Aw, "Kinematic design optimization of a parallel ankle rehabilitation robot using modified genetic algorithm," *Robot. Auton. Syst.* **57**(10), 1018–1027 (2009).

https://doi.org/10.1017/S0263574714001945 Published online by Cambridge University Press